Applied Catalysis B: Environmental 242 (2019) 293–301

Contents lists available at ScienceDirect

Applied Catalysis B: Environmental

journal homepage: www.elsevier.com/locate/apcatb

Efficient visible light driven hydrogen generation using 9-(3,3-dimethyl-1,2-oxazetidine-*N*-yl)perylene-3,4-dicarboximide functionalized amino graphene

Kalyanasundaram Abinaya[a], Samuvelnesamani Karthikaikumar[a], Kaliyaperumal Sudha[a], Subramani Sundharamurthi[a], Arumugam Elangovan[b], Palanisamy Kalimuthu[a,*]

[a] Department of Chemistry, The Gandhigram Rural Institute-Deemed to be University, Gandhigram, Dindigul, 624302, Tamilnadu, India
[b] Department of Chemistry, Thiagarajar College, Madurai, 625009, Tamilnadu, India

ARTICLE INFO

Keywords:
Photocatalyst
Push-pull perylene
Perylene-graphene hybrid
Hydrogen generation
Sacrificial donor

ABSTRACT

Synthesis of oxazetidine substituted perylene dye *N*-(2,5-di-tert-butylphenyl)-9-(3,3-dimethyl-1,2-oxazetidine-*N*-yl)perylene-3,4-dicarboximide is reported. The imide moiety present in the reported dye was used to functionalize amino graphene. The 9-(3,3-dimethyl-1,2-oxazetidine-*N*-yl) perylene-3,4-dicarboximide was used as light harvester for photocatalytic hydrogen generation by covalently attaching on to amino graphene surface. The composite AG-DOPMI/Pt was prepared and found to be an efficient photocatalyts for hydrogen production from methanol:water mixture which can produce 1489 μmol/g hydrogen. The oxazetidine dye gives rise to the production of hydrogen generation even in the absence of sacrificial donor.

1. Introduction

Perylene is a photostable compound which has high molar extinction coefficient along with broad optical window [1,2]. Perylene derivatives have been utilized for several applications depending on its structural modifications [3–7]. The optical absorption of perylene dyes can be shifted or widened to near-IR region by structural modifications which is achieved through functionalizing its different positions [8–10]. They find various applications in light emitting diode, dye sensitized solar cells, supramolecular chemistry due to its long lasting fastness, light harvesting ability, thermal and photochemical stability [11–13].

Initial development of perylene derivatives are perylene diimides which have been used as building blocks for constructing electronic and optoelectronic devices such as dye lasers, organic light emitting diodes, optical switches and photodetectors [14–17]. Then bay substitution of perylene with bulkier substituents were developed to avoid π–π stacking which is favourable in large π aromatic systems [2,9]. Push-pull type of perylene dyes were introduced by substituting donor and acceptor units at opposite ends of perylene core [18–20]. This push-pull perylene dyes were widely investigated for its efficient intramolecular charge transfer ability which find applications in solar energy conversion [21–23]. Perylene derivatives have been used as light harvesting materials along with semiconductors for solar energy conversion techniques [18,24–26].

Photocatalytic hydrogen generation is one of the solar energy conversion techniques used to generate hydrogen in an eco-friendly way since it was first reported by Fujishima and Honda in 1972 [27]. Later several modifications have been reported based on varying the photocatalyst to enhance the efficiency of the method [28,29]. Graphene is one such material which has shown improved efficiency as electron transfer mediator in solar energy conversion especially for photocatalytic hydrogen generation by modifying its surface [30–41]. Janarthanan et al have coupled perylene diimide – cobalt complex to graphene scaffold through π–π stacking and proved it as an active platform for hydrogen evolution by mimicking natural photosynthesis [42]. But the covalent functionalization of graphene with dye molecules improves efficiency of the material [43–45].

The modification of graphene through covalent bonds can enrich graphene with various novel physicochemical properties depending on the nature of the added organic functionalities [43]. These graphene hybrids were widely investigated for photocatalytic hydrogen generation, due to the ability of dye unit to harvest solar energy in the visible region whereas the graphene can act as an excellent electron mediator [37]. The back electron transfer reaction occurs in photocatalytic systems, which affects the quantum yield of hydrogen production which was reduced by the usage of sacrificial donor [46–49].

* Corresponding author.
E-mail address: pakalimuthu@gmail.com (K. Palanisamy).

https://doi.org/10.1016/j.apcatb.2018.09.098
Received 13 June 2018; Received in revised form 25 September 2018; Accepted 30 September 2018
Available online 02 October 2018
0926-3373/

Here we report oxazetidine substituted push-pull perylene attached amino graphene for visible light driven hydrogen generation. Newly synthesized 9-(3,3-dimethyl-1,2-oxazetidine-*N*-yl) perylene 3,4-dicarboxylic anhydride (DOPDA) is attached to amino graphene (AG) through covalent bond and utilized this hybrid material (AG-DOPMI) as photocatalyst for hydrogen generation after converting into a platinum composite (AG-DOPMI/Pt).

2. Experimental section

2.1. Materials and methods

Pyrene, HNO_3, ammonia were purchased from Central Drug House, New Delhi for the synthesis of AG according to the procedure reported elsewhere [50]. 3,4,9,10-perylenetetracarboxylic dianhydride, 2,5-di-tert-butyl aniline, zinc acetate dihydrate, imidazole, bromine and 2-amino-2-methyl-1-propanol were purchased from Sigma Aldrich and H_2SO_4, *t*-butanol, glacial acetic acid, KOH and *N*,*N*'-dimethyl formamide (DMF) were purchased from Central Drug House, New Delhi for the synthesis of *N*-(2,5-di-tert-butylphenyl)-9-(3,3-dimethyl-1,2-oxazetidine-*N*-yl)perylene-3,4-dicarboximide (DOPMI) and DOPDA. Silica gel, $CHCl_3$ and petroleum ether were purchased from Central Drug House, New Delhi and the solvents were distilled before use. Ethanol was purchased from Hayman Ltd., UK and H_2PtCl_6 was purchased from Sigma Aldrich for the preparation of platinum composite. All other chemicals were used without further purification. Deionized water was used wherever necessary throughout the experiment. Column chromatography was used to purify compounds at each and every step of organic synthesis, in which silica gel 60–120 mesh was used as stationary phase.

2.2. Characterization

^1H and ^{13}C NMR measurements were carried out with BRUKER 400 MHz NMR spectrometer using trimethylsilane as internal standard. UV–vis spectral measurements were obtained for the synthesized materials using Perkin-Elmer Lamda 35 spectrophotometer. Fourier transform infrared (FT-IR) spectra were recorded for the synthesized materials with JASCO FT-IR 460 plus model spectrometer. The elemental composition of AG-DOPMI was investigated by X-ray Photoelectron Spectroscopy (XPS) using PHI 5000 Versa Probe II, FEI Inc and powder X-ray diffraction (PXRD) measurements for the materials were made using X'PER-PRO model PANalytical. Scanning electron microscopic (SEM) and EDX mapping studies were conducted on a Vega 3 Tescon microscope operated at 10.0 kV for analyzing the surface morphology of synthesized materials. Thermogravimetric analysis (TGA) of AG-DOPMI was conducted using thermogravimetric analyzer made of Shimadzu TGA-50 series model in nitrogen atmosphere. The photocatalytic hydrogen generation of AG-DOPMI loaded with platinum nanoparticles was analysed by gas chromatography made of Perkin Elmer, Clarus 500 model equipped with thermal conductivity detector (GC-TCD) using 13× molecular sieve column and argon as carrier gas. Inductively coupled plasma – mass spectroscopy (ICP-MS) measurement was made to analyse the amount of platinum deposited in AG-DOPMI/Pt using Thermo Scientific, iCAP RQ model and the experimental details are given in Supplementary material. Elemental analysis of the samples were made using Truspec Micro Analyser made.

The electrochemical studies were carried out under nitrogen atmosphere using CHI Model 760D electrochemical workstation. The electrochemical measurements were carried out using two component three electrode cell using Ag/AgCl as reference electrode and platinum wire as counter electrode in a 0.1 M KCl medium. And the working electrode is 0.1 g/mL of AG and AG-DOPMI aqueous suspension drop casted on glassy carbon electrodes. The carbon electrodes were cleaned using 0.5 μm and 0.05 μm alumina slurry followed by sonication before drop casting. Differential pulse voltammetry studies were done with a pulse width of 0.05 s and an amplitude of 0.06 V.

2.3. Photocatalytic hydrogen generation

The photocatalytic hydrogen generation of hybrid material composed of amino graphene, 9-(3,3-dimethyl-1,2-oxazetidine-*N*-yl)perylene-3,4-dicarboximide and platinum (AG-DOPMI/Pt) was carried out using borosilicate type glass vial of 28 mL with an inner diameter of 4 cm and 85% transparency for 350 nm to 1100 nm. 10 mg of AG-DOPMI/Pt is suspended in 10 mL of methanol-water mixture of 2:8 v/v ratio. The atmospheric and the dissolved oxygen were removed by purging with dry nitrogen gas. Then the light of wavelength from 420 nm was allowed to pass through the bottom of the vial from Xenon lamp source fitted with 420 nm cut-off filter (Newport; 300 W). To maintain the temperature of the vial below 50 °C, it was kept 10 cm away from the source in a strong current of air. A Gas chromatograph equipped with 13× molecular sieve column with argon as carrier gas and thermal conductivity detector was used to analyse the hydrogen gas. 100 μL of the gas samples from the vial was injected in the GC using syringe. The known concentrations of standard H_2/N_2 gas mixtures were used for calibrating GC signal. The sample vials were replenished with methanol:water mixture in every cycle for cycling measurements. Further the apparent quantum efficiency (AQE) of the synthesized material was calculated by using the number of incident photons and the number of reacted electrons as given in following equations [51].

$$AQE = \frac{number\ of\ reacted\ electrons}{number\ of\ incident\ photon}\ x\ 100$$

$$AQE = \frac{2\ x\ number\ of\ H_2\ molecules\ evolved}{number\ of\ incident\ photon}\ x\ 100$$

2.4. Synthesis of N-(2,5-di-tert-butylphenyl)-9-(3,3-dimethyl-1,2-oxazetidine-N-yl) perylene-3,4-dicarboximide (DOPMI)

N-(2,5-di-tert-butylphenyl)perylene-3,4-dicarboximide (PMI) and 9-bromo-*N*-(2,5-di-tert-butylphenyl)perylene-3,4-dicarboximide (BRPMI) were synthesized according to the procedure reported elsewhere [52]. For the synthesis of DOPMI, 400 mg (0.680 mmol) of 9-bromo-*N*-(2,5-di-tert-butylphenyl)perylene-3,4-dicarboximide (BRPMI) was dissolved in 25 mL of dry DMF by stirring and the reaction mixture was degassed with nitrogen. Then 1.95 mL (20.4 mmol) of 2-amino-2-methyl-1-propanol was added and heated under nitrogen atmosphere at 100 °C for 5 h. After cooling the reaction mixture to room temperature, the crude product was extracted with $CHCl_3$, distilled and dried with $MgSO_4$. The product was purified by column chromatography using 2:3 $CHCl_3$: pet ether solvent ratio. The ^1H NMR spectrum of DOPMI is shown in Fig. S1. ^1H NMR ($CDCl_3$): 8.61 δ, 1H, d, 8.0 Hz; 8.59 δ, 1H, d, 8.0 Hz; 8.46 δ, 1H, d, 8.0 Hz; 8.38 δ, 1H, d, 8.0 Hz; 8.37 δ, 1H, d, 8.0 Hz; 8.29 δ, 2H, d, 8.0 Hz; 7.64 δ, 1H, d, 8.0 Hz; 7.59 δ, 1H, t, 8.0 Hz; 7.18 δ, 1H, d, 8.0 Hz; 7.44 δ, 1H, dd, 2.08 Hz, 6.48 Hz; 7.02 δ, 1H, d, 8.0 Hz; 3.05 δ, 6H, s; 1.33 δ, 9H, s; 1.30 δ, 9H, s. Anal. Calcd for $C_{41}H_{42}N_2O_3$ (610.32): C, 80.62%; H, 6.93%; N, 4.59%. Found: C 80.57%; H, 6.89%; N, 4.51%.

2.4.1. Synthesis of 9-(3,3-dimethyl-1,2-oxazetidine-N-yl) perylene 3,4-dicarboxylic anhydride (DOPDA)

50 mg (0.08 mmol) of *N*-(2,5-di-tert-butylphenyl)-9-(3,3-dimethyl-1,2-oxazetidine-*N*-yl)perylene-3,4-dicarboximide was dissolved in 15 mL of *t*-butanol. Then 203 mg (3.62 mmol) KOH was added and heated under stirring at 80 °C for 2 h. Then it was poured into 50 mL glacial acetic acid and stirred for 15 min. The crude product was extracted with $CHCl_3$, distilled and dried with $MgSO_4$. The product was purified by column chromatography using 20:80 ethylacetate:pet ether solvent ratio. The ^1H NMR spectrum of DOPDA is shown in Supplementary material Fig. S3. ^1H NMR (d-DMSO): 8.74 δ, 1H, d, 7.2 Hz; 8.64 δ, 1H, d, 7.6 Hz; 8.62 δ, 1H, d, 8.4 Hz; 8.52 δ, 1H, d, 8.0 Hz;

8.42 δ, 1H, d, 8 Hz; 8.39 δ, 1H, d, 8.0 Hz; 8.28 δ, 1H, d, 8.8 Hz; 7.73 δ, 1H, t, 8.0 Hz; 7.25 δ, 1H, d, 8.4 Hz; 5.77 δ, 2H, s; 3.03 δ, 6H, s. Anal. Calcd for $C_{26}H_{17}NO_4$ (407.42): C, 76.65; H, 4.21; N, 3.44; Found: C, 76.57%; H, 4.19%; N, 3.36%.

2.5. Preparation of AG-DOPMI /Pt and AG/Pt

Preparation of AG-DOPMI involves two steps. The first step is the preparation of AG by following the procedure reported elsewhere [50]. The second step is the covalent attachment of DOPDA to AG as follows, 500 mg of AG, 50 mg (0.1 mmol) of DOPDA and 15 mg K_2CO_3 were dispersed in 20 mL of dry DMF. The solution was deaerated with nitrogen to remove dissolved oxygen and heated to 90 °C for 2 days with constant stirring. Then the product was washed with DMF to remove excess DOPDA and dried under vacuum for 24 h. The surface of both AG and AG-DOPMI was modified with Pt cocatalyst by typical ethanol reduction method reported elsewhere [53].

The procedure involves initially the heating of 50 mg of aqueous AG-DOPMI in 10 mL of water ethanol mixture (v/v = 2/1) to 70 °C along with 0.4 mL of aqueous solution of H_2PtCl_6 (8 mmol). Then the pH of the reactant mixture was adjusted to 10 using potassium hydroxide. Finally the solution was refluxed for 10 h under constant stirring. The product was cooled, washed with water and dried under vacuum for 24 h. 0.66 µg of platinum was deposited on AG-DOPMI which is confirmed from the ICP-MS analysis.

3. Results and discussion

3.1. Structure and morphology

The structure of DOPMI and DOPDA were well established using NMR spectra and were presented in their synthesis sections. But the structure of AG-DOPMI and AG-DOPMI/Pt were analysed with the help of FT-IR, XRD and XPS analysis as follows. The FT-IR spectra of AG-DOPMI was compared with AG, DOPDA and DOPMI as shown in Fig. 1 to confirm the formation of AG-DOPMI. The skeletal vibrations of AG occurred between 900 and 1780 cm^{-1} as found in Fig. 1c matches with the vibrational bands in Fig. 1a which confirms the presence of AG moiety in AG-DOPMI. The signature of the skeletal vibrational bands of DOPMI from 700 to 1700 cm^{-1} (Fig. 1b) were merged with the vibrational bands of AG. Besides, the peak corresponds to the free amino group in AG-DOPMI at 3231 cm^{-1} is also present.

The vibrational bands of anhydride are shifted from 1755 cm^{-1} to 1700 cm^{-1} after conversion to imide group as shown in the FT-IR spectra of DOPDA and DOPMI. Similarly the absence of peak at 1755 cm^{-1} and the appearance of peak at 1568 cm^{-1} which is hidden in the skeletal vibrations of AG confirms the formation of AG-DOPMI

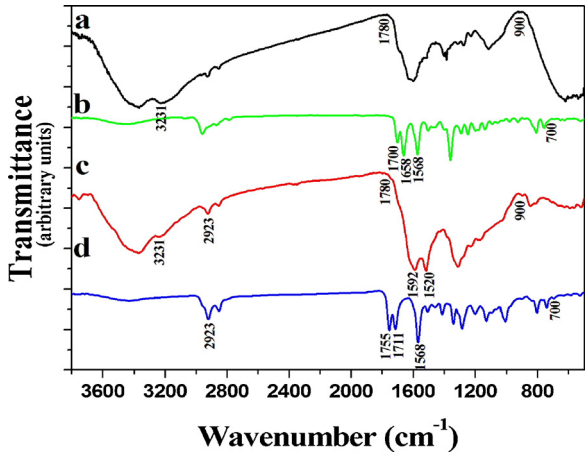

Fig. 1. FT-IR spectra of (a) AG, (b) DOPMI, (c) AG-DOPMI and (d) DOPDA.

(Scheme 2). Thus the structure of AG-DOPMI proposed in scheme 1 is well supported by these vibrational bands obtained from FT-IR spectra.

The PXRD measurements of AG, AG-DOPMI and AG-DOPMI/Pt were made to understand the crystallinity of the synthesized materials that are shown in Fig. 2. The sharp peak at 2θ value of 26° in Fig. 2a is attributed to AG [50]. It can also be well seen in the PXRD spectra of AG-DOPMI and AG-DOPMI/Pt in Fig. 2b and 2c and further supports the confirmation of the presence of AG unit in AG-DOPMI and AG-DOPMI/Pt. The peaks present from 10° to 25° in AG-DOPMI confirm the presence of perylene unit similar to perylene monoimide as shown in Fig. 2d. The PXRD spectrum of AG-DOPMI/Pt (Fig. 2c) reveals the loading of platinum on AG-DOPMI.

The appearance of the peaks at 2θ values 39.5°, 46.2° and 67.5° in AG-DOPMI/Pt (Fig. 2c) corresponds to the crystalline planes such as (111), (220) and (200) of face centered cubic platinum in addition to the diffraction peaks of AG-DOPMI confirms the presence of platinum in AG-DOPMI/Pt [54]. Further the EDX spectrum of AG-DOPMI/Pt (Fig. 6a and 6b) supports the deposition of platinum. XPS analysis was used to demonstrate the elemental composition of AG-DOPMI. The survey spectrum of AG-DOPMI (Fig. 3) contains elements such as C, N and O.

The N1s core level XPS spectrum (Fig. 4a) has two peaks in which the peak centered at 397.5 eV is further resolved into two peaks. The deconvoluted peak of N1s core at 399.9 eV in Fig. 4a is ascribed to the presence of imide nitrogens [55]. Another peak at 397.5 eV in Fig. 4a is attributed the presence of nitrogen in the form of free $-NH_2$ group in AG-DOPMI [56]. The peak centered at 404 eV corresponds to the nitrogen atom (> N−O) present in the oxazetidine ring [57]. These results reveal that three types of nitrogen atoms are present in AG-DOPMI, which confirms the presence of oxazetidine unit in perylene moiety, free amino group present in AG moiety and imide group that links perylene and AG together. Similarly, the two deconvoluted peaks are shown in Fig. 4b correspond to O1s core level reveals the presence of two types of oxygen atoms in AG-DOPMI. The presence of > C═O groups of AG-DOPMI is confirmed from the deconvoluted peak of O1s core at 529.5 eV and the other peak centered at 531.5 eV is contributed to the presence of oxygen atom present in (−C−O−C) unit of physically bound DOPDA on AG [58].

SEM images of AG, AG-DOPMI and AG-DOPMI/Pt were obtained to examine the surface morphology of synthesized materials. Fig. 5a and b reveals that the aggregation of AG does not have any significant change even after functionalization of AG with DOPDA.

Further Fig. 5b shows that both AG and AG-DOPMI were not present as uniformly sized particles. This is probably due to the aggregation which arises as a result of π-π stacking between individual moieties of AG and AG-DOPMI. The deposition of Pt on AG-DOPMI layers increases the aggregation which has clump of particles of AG-DOPMI which is evident from Fig. 5c. This may be attributed to aggregation enhanced by Pt nanoparticles due to the intercalation of platinum nanoparticles between AG-DOPMI layers.

Energy dispersive X-ray (EDX) studies were performed to analyze the elements present in the synthesized materials AG-DOPMI and AG-DOPMI/Pt (Fig. 6a and b). The EDX spectrum in Fig. 6a shows the presence of carbon, nitrogen and oxygen in AG-DOPMI. Whereas EDX spectrum of AG-DOPMI/Pt (Fig. 6b) shows the presence of platinum in addition to carbon, nitrogen and oxygen. Hence the EDX spectrum further proves the deposition of platinum on AG-DOPMI in AG-DOPMI/Pt. The amount of platinum deposited on AG-DOPMI was quantified using ICP-MS. It was estimated that 0.66 µg of platinum was deposited per gram of AG-DOPMI.

3.2. Thermal stability analysis

The thermal stability of the synthesized material AG-DOPMI was understood by thermogravimetric analysis under nitrogen atmosphere and the thermogram is shown in Fig. 7. It shows that upon gradual

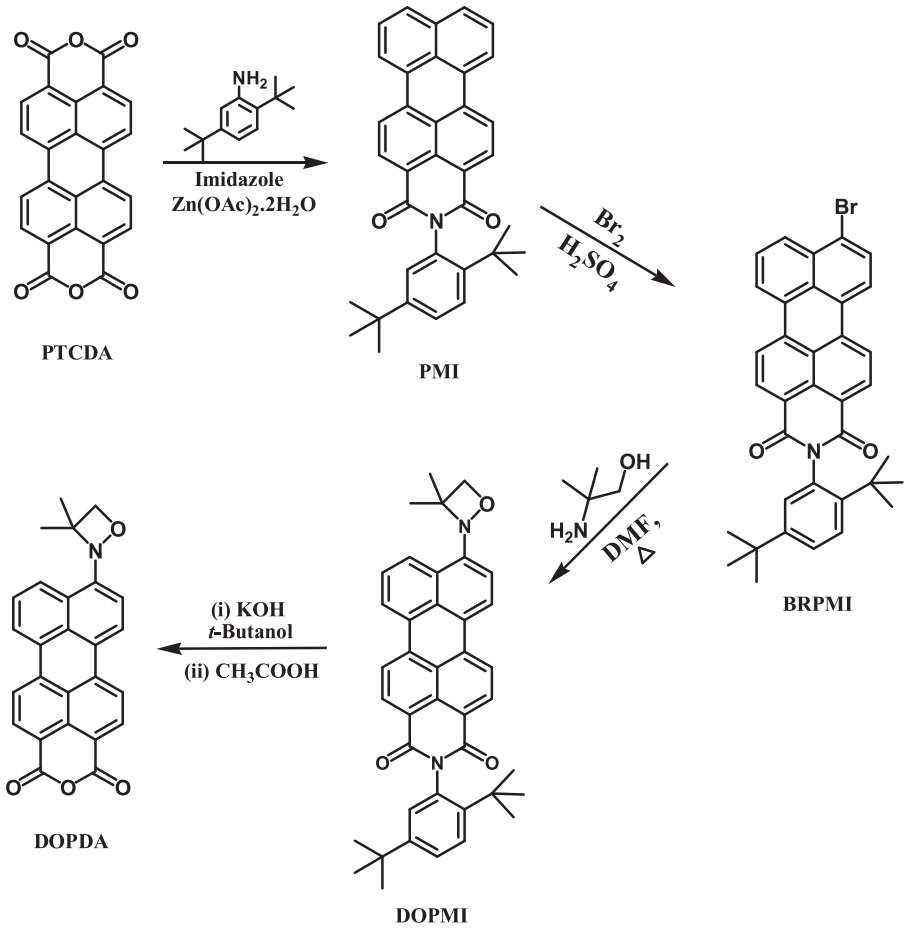

Scheme 1. Synthetic scheme of DOPDA.

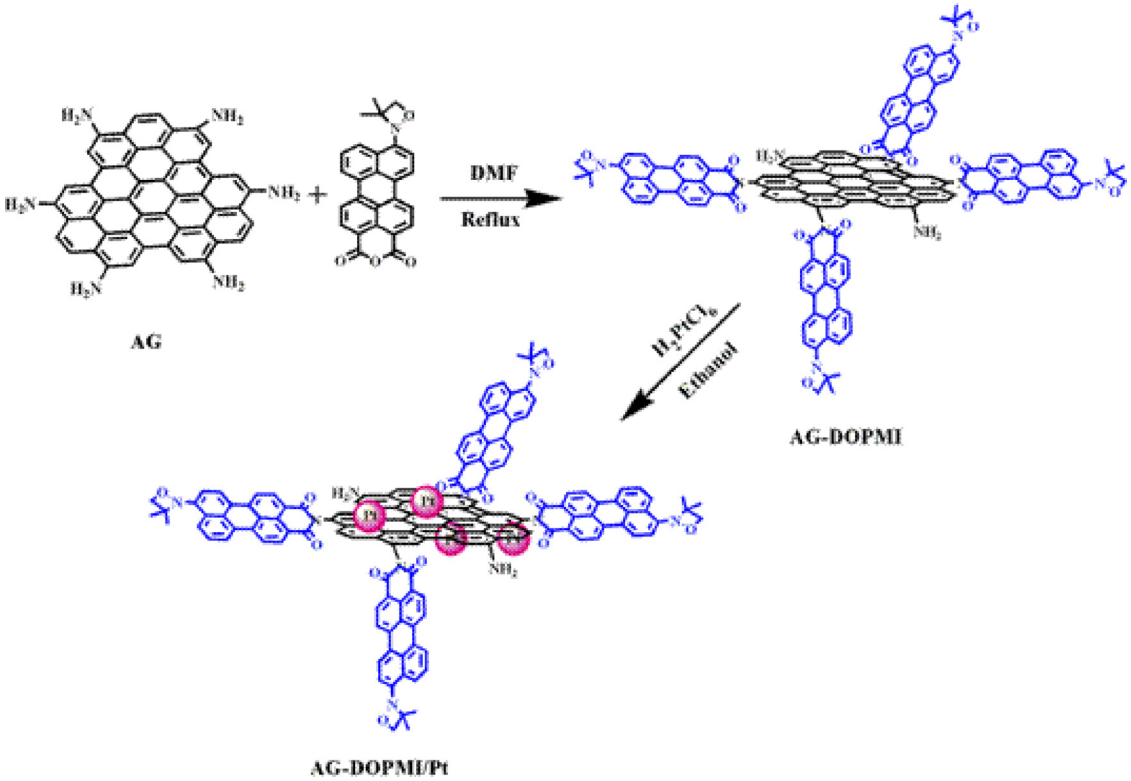

Scheme 2. Schematic representation of the synthetic route of AG-DOPMI/Pt.

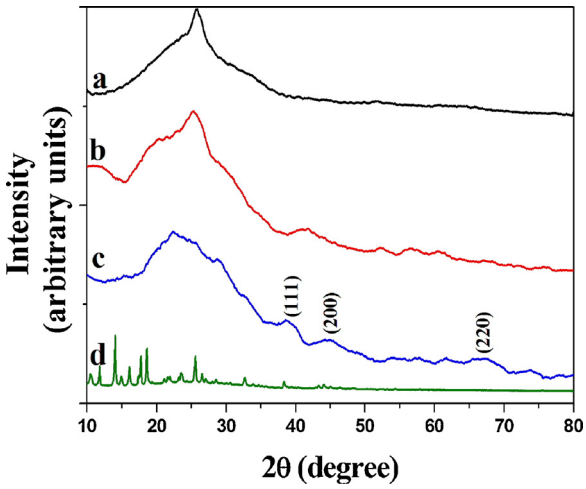

Fig. 2. XRD spectra of (a) AG, (b) AG-DOPMI, (c) AG-DOPMI/Pt and (d) PMI.

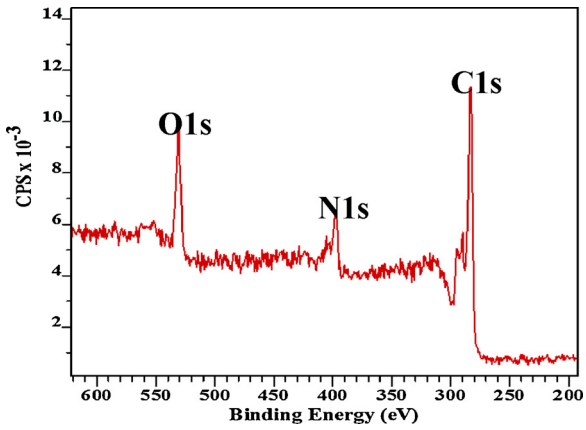

Fig. 3. XPS survey spectrum of AG-DOPMI.

increase of temperature, weight loss (3.5%) at 120 °C is occurred due to the trace of water molecules trapped in AG-DOPMI. The decomposition of perylene and graphene units was occurred between 430 and 580 °C. It shows that the AG-DOPMI can be stable up to 400 °C and this allows the material to operate at high temperatures.

3.3. Optical properties

The UV–vis absorption spectra of AG, DOPMI and AG-DOPMI is shown in Fig. 8. UV–vis spectrum of AG has maximum absorption features at 360 and 465 nm whereas DOPMI has absorption maximum at 550 nm. By attaching DOPMI to AG covalently, the AG-DOPMI has absorption which covers almost entire visible region of solar spectrum from 350 to 850 nm (Fig. 8c). This broad absorption of AG-DOPMI is due to the π–π^*, n–π^* and charge transfer transitions which occurs in graphene, and DOPMI moieties as seen in Fig. 8a and b. And the widening of spectral window in AG-DOPMI upto 850 nm accounts for the feasible electronic conjugation between DOPMI and AG. This broadened optical window of AG-DOPMI proves that this material can harvest visible light upto 850 nm. This spectral broadening is a pre-requisite for materials of photocatalytic hydrogen generation. Since the solar radiation on earth has spectral window which extends upto Near IR region.

3.4. Photocatalytic activity of AG-DOPMI/Pt

Photocatalytic hydrogen generation was carried out using AG-DOPMI/Pt in water as well as 20% methanol aqueous system. The photocatalytic activity of AG-DOPMI/Pt in 2:8 methanol:water mixture (Fig. 9a) shows that it can produce 1489 μmol g^{-1} of hydrogen after 5 h of visible light illumination. Whereas AG/Pt in 2:8 methanol:water mixture (Fig. 9c) shows only 230 μmol g^{-1} of hydrogen generation upon same illumination time. This 6.4 fold increase in the hydrogen generation upon functionalization of AG with DOPMI is attributed to the wide spectral window of AG-DOPMI (vide supra). The widened spectral window of AG-DOPMI compared to that of AG proves that it can capture the light upto 850 nm. This superior light harvesting ability of AG-DOPMI accounts for the increase in its photocatalytic hydrogen generation ability. Further the effect of functionalization of AG was investigated by analyzing the photocatalytic activity of AG-DOPMI/Pt in the absence of methanol (sacrificial donor).

The results in Fig. 9b clearly show that AG-DOPMI/Pt produces 940 μmol g^{-1} of hydrogen in the absence of sacrificial donor on 5 h of visible light illumination. The significant hydrogen generation of AG-DOPMI/Pt in the absence of sacrificial donor accounts for the efficiency of oxazetidine unit present in DOPDA. Hence the oxazetidine unit present in DOPDA will act as in-situ sacrificial donor to quench the hole generated in AG-DOPMI/Pt upon illumination. The enhanced photocatalytic hydrogen generation of AG-DOPMI/Pt proves that the oxazetidine unit present in DOPDA act both as an electron donor as well

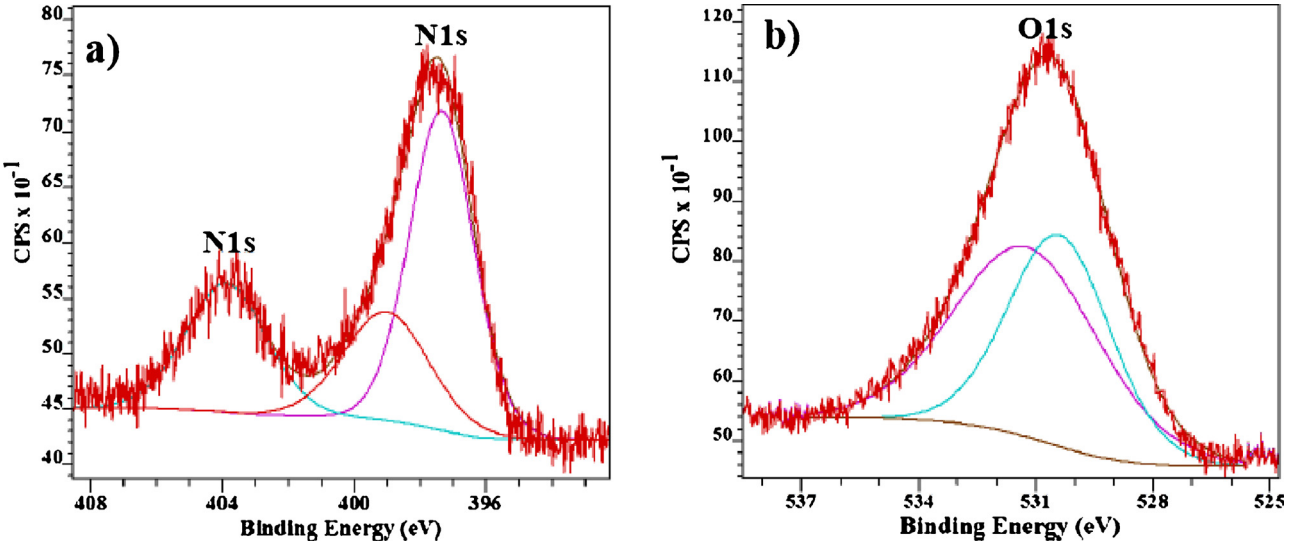

Fig. 4. XPS spectra of AG-DOPMI (a) N1s (b) O1s deconvoluted peaks.

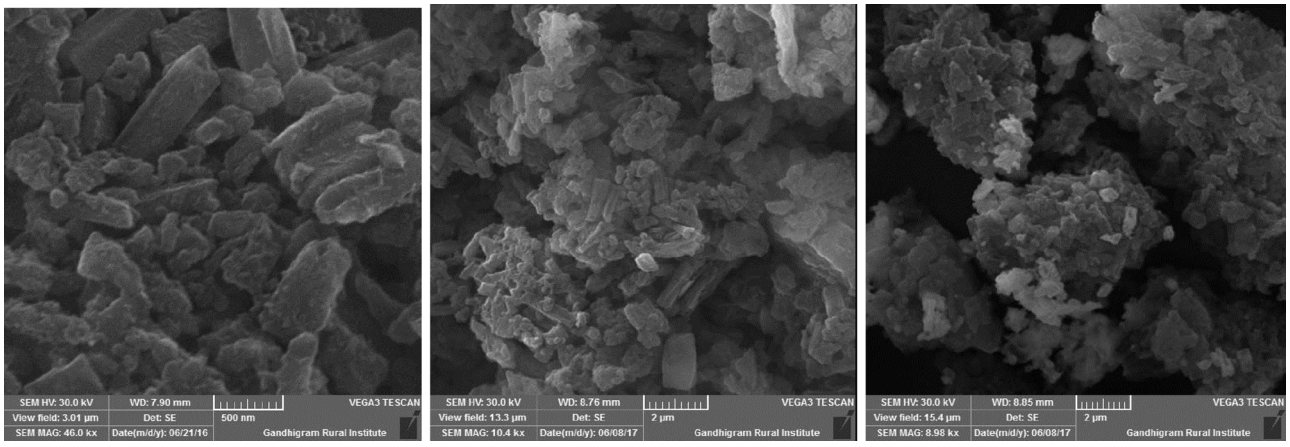

Fig. 5. SEM image of (a) AG, (b) AG-DOPMI and (c) AG-DOPMI/Pt.

as hole quencher. This proves that the introduction of oxazetidine unit in the perylene monoimide of photocatalyst will be the efficient composite for enhance the photocatalytic hydrogen production from methanol:water mixture.

Besides, the photocatalytic reaction mechanism of AG-DOPMI/Pt is further confirmed with the electrochemical studies. The energy levels obtained from electrochemical studies are summarized in Table 1 and it proves that the transfer of photo-induced electron is feasible from LUMO of AG-DOPMI to platinum (Fig. 11). The apparent quantum efficiency (AQE) was calculated for the AG-DOPMI/Pt from 420 to 850 nm and is shown in Fig. 10. The maximum AQE of 4.26% was obtained at 520 nm.

Further The photocatalytic hydrogen generation of AG-DOPMI in the absence of sacrificial donor gives 940 µmol/g of hydrogen. This is in contrast to the hydrogen generation of AG (232 µmol/g) in the presence of sacrificial donor. And the 1.6 fold decrease in photocatalytic hydrogen generation of AG-DOPMI/Pt in the absence of methanol shows the significance of sacrificial donor to regenerate the material which was oxidized upon visible light illumination. Hence the hydrogen generation of AG-DOPMI in the absence of sacrificial donor accounts for the effect of oxazetidine unit introduced in DOPMI moiety. Moreover the maximum AQE of AG-DOPMI/Pt obtained at 535 nm is shown in Fig. 10 [58].

The stability of AG-DOPMI/Pt was confirmed by measuring the hydrogen generation of AG-DOPMI/Pt upon illumination with visible light source which is shown in Fig. 12a. The amount of hydrogen produced by AG-DOPMI/Pt in the presence of 20% of methanol as well as in the absence of methanol on visible light illumination is shown in Fig. 12b. Fig. 12b proves that the photocatalytic hydrogen generation of AG-DOPMI/Pt in the presence of 20% methanol remains constant even

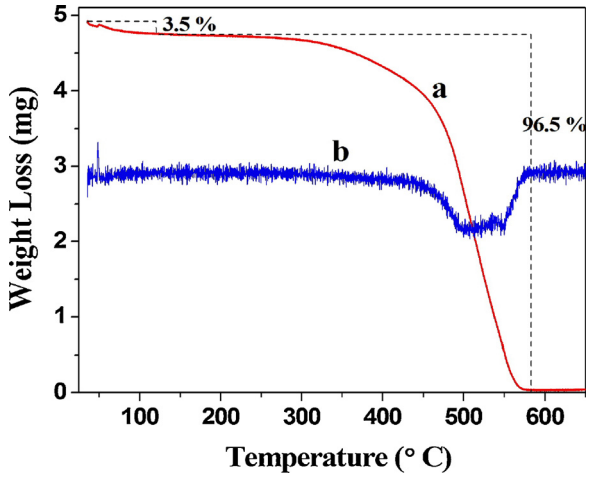

Fig. 7. (a) Thermogram of AG-DOPMI and (b) its first derivative curve.

after several cycles. This shows that the AG-DOPMI/Pt is an efficient composite for photocatalytic hydrogen generation. Contrarily, the photocatalytic hydrogen generation of AG-DOPMI/Pt from water without methanol has decreased to 429 µmol/g. The 2 fold decrease in the photocatalytic hydrogen generation of AG-DOPMI/Pt without methanol after several cycles of visible light illumination shows that the efficiency of the material decreases. This decreasing efficiency of AG-DOPMI/Pt without methanol shows that the material gets oxidized upon visible light illumination and the oxidized material is in need of a sacrificial donor (methanol) to regenerate the photocatalyst.

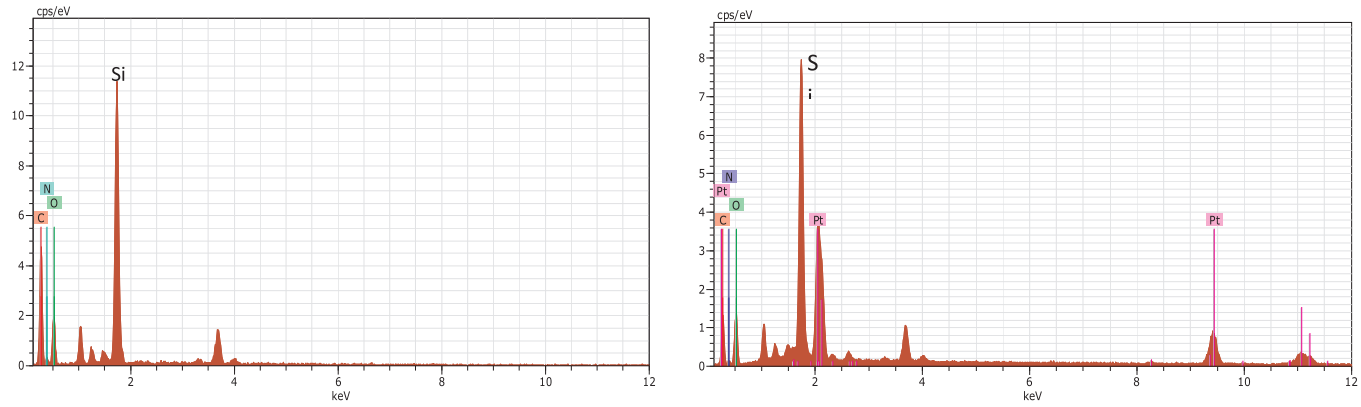

Fig. 6. EDX spectrum of (a) AG-DOPMI and (b) AG-DOPMI/Pt.

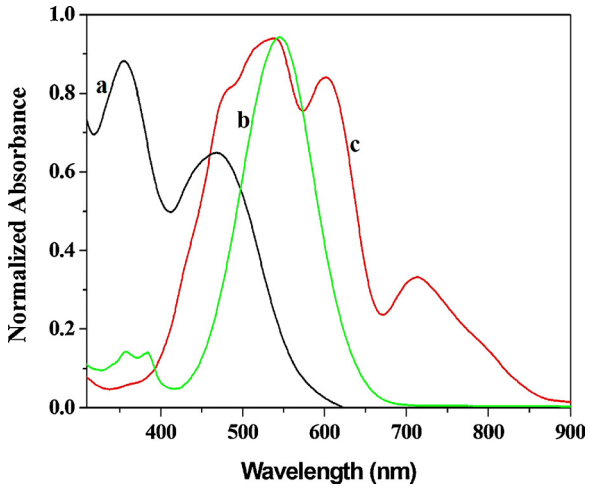

Fig. 8. UV–vis spectra of (a) AG, (b) DOPMI and (c) AG-DOPMI.

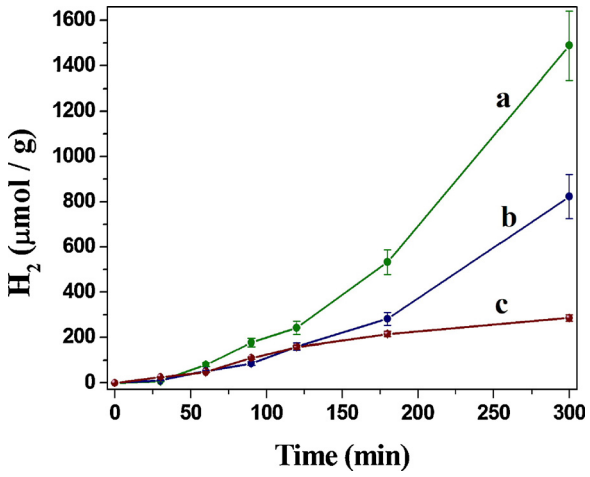

Fig. 9. Photocatalytic hydrogen generation of (a) AG-DOPMI/Pt with methanol:water (2:8) mixture (b) AG-DOPMI/Pt without methanol and (c) AG/Pt with methanol:water (2:8) mixture.

Table 1
Energy level parameters of AG-DOPMI and AG.

Compound	E_{ox}^{onset} (V)	λ_{max}^{onset} (nm)	E_g (eV)	HOMO (eV)	LUMO (eV)
AG-DOPMI	1.78	853	1.45	−6.20	−4.75
AG	1.37	700	1.77	−5.79	−4.02

$E_g = 1240/\lambda_{onset}$; E_{HOMO} (eV) $= -[E_{ox}^{onset} + 4.8 - E_{Fc/Fc+}]$; E_{LUMO} (eV) $= E_g + E_{HOMO}$ (eV).

4. Conclusion

An oxazetidine unit has been successfully introduced in a perylene dye as an efficient donor unit. Further the dye was converted into a hybrid composite material using AG and platinum. The composite AG-DOPMI/Pt was found to be an efficient photocatalyts for hydrogen production from methanol:water mixture which can produce 1489 μmol/g hydrogen. 6.4 fold increases in the hydrogen generation upon functionalization of AG with DOPMI was found. Moreover the oxazetidine group in DOPMI not only enhances the light harvesting ability of AG-DOPMI/Pt but also stimulates the photocatalytic hydrogen generation (940 μmol/g) even in the absence of sacrificial donor.

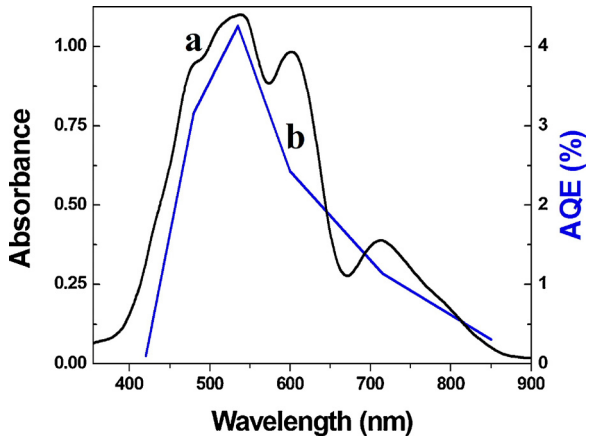

Fig. 10. (a) Absorption spectrum and (b) apparent quantum efficiency of AG-DOPMI.

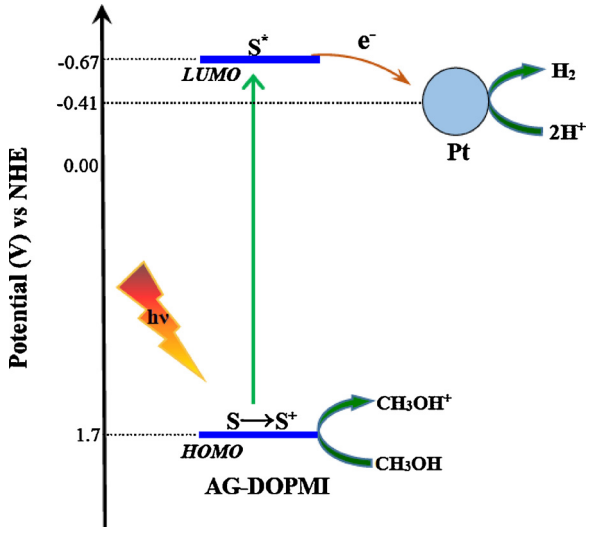

Fig. 11. Schematic representation for the photocatalytic hydrogen generation by AG-DOPMI.

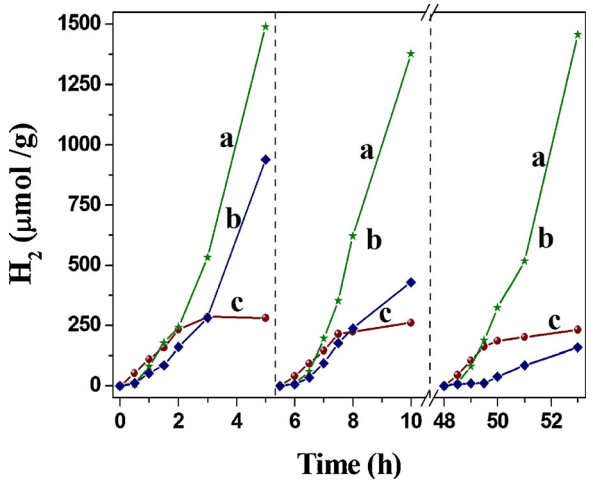

Fig. 12. Recycling measurements for photocatalytic hydrogen generation of (a) AG-DOPMI/Pt with methanol:water (2:8) mixture (b) AG-DOPMI/Pt without methanol and (c) AG/Pt with methanol:water (2:8) mixture.

Acknowledgment

KA and PK gratefully acknowledgeUniversity Grants Commission, New Delhi for providing financial support through UGC-MRP (F.No. 41-251/2012(SR)). The authors also sincerely acknowledge the NMR Facility created under DST-FIST programme (SR/FST/CSI-255/2013(C) dtd: 23.04.2015) for recording NMR spectra.

Appendix A. Supplementary data

Supplementary material related to this article can be found, in the online version, at doi:https://doi.org/10.1016/j.apcatb.2018.09.098.

References

[1] C. Li, Z. Liu, J. Schoneboom, F. Eickemeyer, N.G. Pschirer, P. Erk, et al., Perylenes as sensitizers in hybrid solar cells: how molecular size influences performance, J. Mater. Chem. 19 (2009) 5405–5415.
[2] C. Li, J. Schöneboom, Z. Liu, N.G. Pschirer, P. Erk, A. Herrmann, et al., Rainbow perylene monoimides: easy control of optical properties, Chem.—A Eur. J. 15 (2009) 878–884.
[3] Y. Li, C. Wang, C. Li, S. Di Motta, F. Negri, Z. Wang, Synthesis and properties of ethylene-annulated di(perylene diimides), Org. Lett. 14 (2012) 5278–5281.
[4] A. Keerthi, Y. Liu, Q. Wang, S. Valiyaveettil, Synthesis of perylene dyes with multiple triphenylamine substituents, Chem.—Eur. J. 18 (2012) 11669–11676.
[5] J. Chen, H. Jiao, W. Li, D. Liao, H. Zhou, C. Yu, Real-time fluorescence turn-on detection of alkaline phosphatase activity with a novel perylene probe, Chem.—Asian J. 8 (2013) 276–281.
[6] Z. Zhang, C. Zhan, X. Zhang, S. Zhang, J. Huang, A.D.Q. Li, et al., A self-assembly phase diagram from amphiphilic perylene diimides, Chem.—Eur. J. 18 (2012) 12305–12313.
[7] Y. Shibano, H. Imahori, C. Adachi, Organic thin-film solar cells using electron-donating perylene tetracarboxylic acid derivatives, J. Phys. Chem. C 113 (2009) 15454–15466.
[8] F. Wurthner, Z. Chen, V. Dehm, V. Stepanenko, One-dimensional luminescent nanoaggregates of perylene bisimides, Chem. Commun. (2006) 1188–1190.
[9] L. Xu, C. Liu, Z. Qin, R. Jiang, Y. Li, Core expansion of perylenetetracarboxdiimide dyes with anthraquinone units for electron-accepting materials, Eur. J. Org. Chem. 2013 (2013) 300–306.
[10] Z. Yao, C. Yan, M. Zhang, R. Li, Y. Cai, P. Wang, N-annulated perylene as a coplanar π-linker alternative to benzene as a low energy-gap, metal-free dye in sensitized solar cells, Adv. Energy Mater. 4 (2014) 1400244–n/a.
[11] C. Li, H. Wonneberger, Perylene imides for organic photovoltaics: yesterday, today, and tomorrow, Adv. Mater. 24 (2012) 613–636.
[12] F. Würthner, Perylene bisimide dyes as versatile building blocks for functional supramolecular architectures, Chem. Commun. (2004) 1564–1579.
[13] S. Ferrere, A. Zaban, B.A. Gregg, Dye sensitization of nanocrystalline tin oxide by perylene derivatives, J. Phys. Chem. B 101 (1997) 4490–4493.
[14] A.P. Kulkarni, C.J. Tonzola, A. Babel, S.A. Jenekhe, Electron Transport materials for organic light-emitting diodes, Chem. Mater. 16 (2004) 4556–4573.
[15] G. Wirnsberger, P. Yang, H.C. Huang, B. Scott, T. Deng, G.M. Whitesides, et al., Patterned Block-copolymer-silica mesostructures as host media for the laser dye Rhodamine 6G, J. Phys. Chem. B 105 (2001) 6307–6313.
[16] N. Mizoshita, T. Tani, S. Inagaki, Isothermally reversible fluorescence switching of a mechanochromic perylene bisimide dye, Adv Mater 24 (2012) 3350–3355.
[17] U. Shafique, K.S. Karim, Lateral organic photodetectors for imaging applications. 7961 (2011) 796103–796106.
[18] M. Planells, F.J. Cespedes-Guirao, A. Forneli, A. Sastre-Santos, F. Fernandez-Lazaro, E. Palomares, Interfacial photo-induced charge transfer reactions in perylene imide dye sensitised solar cells, J. Mater. Chem. 18 (2008) 5802–5808.
[19] T. Edvinsson, C. Li, N. Pschirer, J. Schöneboom, F. Eickemeyer, R. Sens, et al., Intramolecular charge-transfer tuning of perylenes: spectroscopic features and performance in dye-sensitized solar cells, J. Phys. Chem. C 111 (2007) 15137–15140.
[20] Q. Qi, X. Wang, L. Fan, B. Zheng, W. Zeng, J. Luo, et al., N-annulated perylene-based push–pull-type sensitizers, Org. Lett. 17 (2015) 724–727.
[21] S. Mathew, H. Imahori, Tunable, strongly-donating perylene photosensitizers for dye-sensitized solar cells, J. Mater. Chem. 21 (2011) 7166–7174.
[22] U.B. Cappel, M.H. Karlsson, N.G. Pschirer, F. Eickemeyer, J. Schöneboom, P. Erk, et al., A broadly absorbing perylene dye for solid-state dye-sensitized solar cells, J. Phys. Chem. C 113 (2009) 14595–14597.
[23] C. Li, J.-H. Yum, S.-J. Moon, A. Herrmann, F. Eickemeyer, N.G. Pschirer, et al., An improved perylene sensitizer for solar cell applications, ChemSusChem 1 (2008) 615–618.
[24] C. Zafer, M. Kus, G. Turkmen, H. Dincalp, S. Demic, B. Kuban, et al., New perylene derivative dyes for dye-sensitized solar cells, Solar Energy Mater. Solar Cells 91 (2007) 427–431.
[25] De Angelis, F. Direct vs, indirect injection mechanisms in perylene dye-sensitized solar cells: a DFT/TDDFT investigation, Chem. Phys. Lett. 493 (2010) 323–327.
[26] C. Zafer, C. Karapire, N. Serdar Sariciftci, S. Icli, Characterization of *N*,*N*-bis-2-(1-hydoxy-4-methylpentyl)-3,4,9,10-perylene bis (dicarboximide) sensitized nanocrystalline TiO_2 solar cells with polythiophene hole conductors, Solar Energy Mater. Solar Cells 88 (2005) 11–21.
[27] A. Fujishima, K. Honda, Electrochemical photolysis of water at a semiconductor electrode, Nature 238 (1972) 37–38.
[28] B. Yan, J. Zhou, X. Liang, K. Song, X. Su, Facile synthesis of flake-like TiO_2/C nanocomposites for photocatalytic H_2 evolution under visible-light irradiation, Appl. Surf. Sci. 392 (2017) 889–896.
[29] F. Cheng, H. Yin, Q. Xiang, Low-temperature solid-state preparation of ternary CdS/g-C_3N_4/CuS nanocomposites for enhanced visible-light photocatalytic H_2-production activity, Appl. Surf. Sci. 391 (2017) 432–439.
[30] X. Li, R. Shen, S. Ma, X. Chen, J. Xie, Graphene-based heterojunction photocatalysts, Appl. Surf. Sci. 430 (2018) 53–107.
[31] Q. Luo, R. Ge, S.-Z. Kang, L. Qin, G. Li, X. Li, Fabrication mechanism and photocatalytic activity for a novel graphene oxide hybrid functionalized with tetrakis-(4-hydroxylphenyl)porphyrin and 1-pyrenesulfonic acid, Appl. Surf. Sci. 427 (2018) 15–23.
[32] H. He, L. Huang, Z. Zhong, S. Tan, Constructing three-dimensional porous graphene-carbon quantum dots/g-C_3N_4 nanosheet aerogel metal-free photocatalyst with enhanced photocatalytic activity, Appl. Surf. Sci. 441 (2018) 285–294.
[33] X. Xu, Z. Si, L. Liu, Z. Wang, Z. Chen, R. Ran, et al., CoMoS2/rGO/C_3N_4 ternary heterojunctions catalysts with high photocatalytic activity and stability for hydrogen evolution under visible light irradiation, Appl. Surf. Sci. 435 (2018) 1296–1306.
[34] K. Lv, S. Fang, L. Si, Y. Xia, W. Ho, M. Li, Fabrication of TiO_2 nanorod assembly grafted rGO (rGO@TiO_2-NR) hybridized flake-like photocatalyst, Appl. Surf. Sci. 391 (2017) 218–227.
[35] D. Liu, Z. Jin, H. Li, G. Lu, Modulation of the excited-electron recombination process by introduce g-C_3N_4 on Bi-based bimetallic oxides photocatalyst, Appl. Surf. Sci. 423 (2017) 255–265.
[36] C. Pu, J. Wan, E. Liu, Y. Yin, J. Li, Y. Ma, et al., Two-dimensional porous architecture of protonated GCN and reduced graphene oxide via electrostatic self-assembly strategy for high photocatalytic hydrogen evolution under visible light, Appl. Surf. Sci. 399 (2017) 139–150.
[37] G. Xie, K. Zhang, B. Guo, Q. Liu, L. Fang, J.R. Gong, Graphene-based materials for hydrogen generation from light-driven water splitting, Adv. Mater. 25 (2013) 3820–3839.
[38] P. Cheng, Z. Yang, H. Wang, W. Cheng, M. Chen, W. Shangguan, et al., TiO_2–graphene nanocomposites for photocatalytic hydrogen production from splitting water, Int. J. Hydrogen Energy 37 (2012) 2224–2230.
[39] D.C.T. Nguyen, J.-H. Woo, K. Youn Cho, C.-H. Jung, W.-C. Oh, Highly efficient visible light driven photocatalytic activities of the $LaCuS_2$-graphene composite-decorated ordered mesoporous silica, Sep. Purif. Technol. 205 (2018) 11–21.
[40] Q. Xiang, J. Yu, M. Jaroniec, Graphene-based semiconductor photocatalysts, Chem. Soc. Rev. 41 (2012) 782–796.
[41] Q. Li, B. Guo, J. Yu, J. Ran, B. Zhang, H. Yan, et al., Highly efficient visible-light-driven photocatalytic hydrogen production of CdS-cluster-decorated graphene nanosheets, J. Am. Chem. Soc. 133 (2011) 10878–10884.
[42] J. Balapanuru, G. Chiu, C. Su, N. Zhou, Z. Hai, Q. Xu, et al., Photoactive PDI–cobalt complex immobilized on reduced graphene oxide for photoelectrochemical water splitting, ACS Appl. Mater. Interfaces 7 (2015) 880–886.
[43] V. Georgakilas, M. Otyepka, A.B. Bourlinos, V. Chandra, N. Kim, K.C. Kemp, et al., Functionalization of graphene: covalent and non-covalent approaches, derivatives and applications, Chem. Rev. 112 (2012) 6156–6214.
[44] B. Xiao, X. Wang, H. Huang, M. Zhu, P. Yang, Y. Wang, et al., Improved superiority by covalently binding dye to graphene for hydrogen evolution from water under visible-light irradiation, J. Phys. Chem. C 117 (2013) 21303–21311.
[45] S. Min, G. Lu, Dye-cosensitized graphene/Pt photocatalyst for high efficient visible light hydrogen evolution, Int. J. Hydrogen Energy 37 (2012) 10564–10574.
[46] T.-F. Yeh, C.-Y. Teng, S.-J. Chen, H. Teng, Nitrogen-doped graphene oxide quantum dots as photocatalysts for overall water-splitting under visible light illumination, Adv. Mater. 26 (2014) 3297–3303.
[47] P.D. Fleischauer, J.K. Allen, Photochemical hydrogen formation by the use of titanium dioxide thin-film electrodes with visible-light excitation, J. Phys. Chem. 82 (1978) 432–438.
[48] W. Zhang, S. Wang, J. Li, X. Yang, Photocatalytic hydrogen production from methanol aqueous solution under visible-light using Cu/S–TiO_2 prepared by electroless plating method, Catal. Commun. 59 (2015) 189–194.
[49] Y.J. Zhang, Y.C. Wang, W. Yan, T. Li, S. Li, Y.R. Hu, Synthesis of Cr_2O_3/TNTs nanocomposite and its photocatalytic hydrogen generation under visible light irradiation, Appl. Surf. Sci. 255 (2009) 9508–9511.
[50] L. Wang, Y. Wang, T. Xu, H. Liao, C. Yao, Y. Liu, et al., Gram-scale synthesis of single-crystalline graphene quantum dots with superior optical propertie, Nat. Commun. 5 (2014) 5357.
[51] Shixiong Min, Gongxuan Lu, Dye-sensitized reduced graphene oxide photocatalysts for highly efficient visible-light-driven water reduction, J. Phys. Chem. C 115 (2011) 13938–13945.
[52] D. Gosztola, M.P. Niemczyk, M.R. Wasielewski, Picosecond molecular switch based on bidirectional inhibition of photoinduced electron transfer using photogenerated electric fields, J. Am. Chem. Soc. 120 (1998) 5118–5119.
[53] X. Li, B. Li, M. Cheng, Y. Du, X. Wang, P. Yang, Catalytic hydrogenation of phenyl aldehydes using bimetallic Pt/Pd and Pt/Au nanoparticles stabilized by cubic silsesquioxanes, J. Mol. Catal. A: Chem. 284 (2008) 1–7.
[54] M. Zhu, Z. Li, B. Xiao, Y. Lu, Y. Du, P. Yang, et al., Surfactant assistance in improvement of photocatalytic hydrogen production with the porphyrin non-covalently functionalized graphene nanocomposite, ACS Appl. Mater. Interfaces 5 (2013) 1732–1740.

[55] Y. Liao, J. Weber, C.F.J. Faul, Fluorescent microporous polyimides based on perylene and triazine for highly CO_2-selective carbon materials, Macromolecules 48 (2015) 2064–2073.
[56] B. Ruelle, S. Peeterbroeck, R. Gouttebaron, T. Godfroid, F. Monteverde, J.-P. Dauchot, et al., Functionalization of carbon nanotubes by atomic nitrogen formed in a microwave plasma Ar + N_2 and subsequent poly(ε-caprolactone) grafting, J. Mater. Chem. 17 (2007) 157–159.
[57] Z. Tehrani, G. Burwell, M.A. Mohd Azmi, A. Castaing, R. Rickman, J. Almarashi, P. Dunstan, A. Miran Beigi, S.H. Doak, O.J. Guy, Generic epitaxial graphene biosensors for ultrasensitive detection of cancer risk biomarker 2D, Materials 1 (2014) 025004.
[58] A.M. Ektessabi, S. Hakamata, XPS study of ion beam modified polyimide films, Thin Solid Films 377–378 (2000) 621–625.